university of groningen / faculty of science and engineering

What makes an alloy shape-memory

Thorough analysis of Ni-Ti R-phase and Ge-Te: Twinning systems and crystallography

Bachelor Integration Project

BSc. Industrial Engineering and Management

ABSTRACT

Shape memory alloys (SMA) play a crucial role in industrial applications, such as in hybrid systems where SMAs are used due to their ability to act simultaneously as sensors and actuators. Martensitic transformation (MT) is the microstructural process that is necessary to obtain SMAs, however, in the literature it is not understood why some alloys are SMA, while others are not despite showing MT. For example, Ni-Ti and Ge-Te show similar martensitic transformations from cubic to R-phase. Despite this fact, Ni-Ti is a SMA, while Ge-Te is not. Therefore, the aim of this research is to explain the differences between these two alloys by thoroughly analysing the microstructure, which will contribute to the further understanding of SMAs. Using crystallographic theories, it is shown that both alloys form compound twinning systems $\{100\}\langle 110\rangle$ and $\{110\}\langle 100\rangle$. Yet, a significant distinction is found in the prediction of the twinning shear in spite of the small discrepancy between the lattice angles. Due to this difference in shear, the crystal structures of both alloys have been further investigated. The results show that the crystal structures of both alloys, despite being similar, have contrasting atomic arrangements inside the crystal cell. This finding, which is often overlooked in the literature, suggests that the macroscopic property of SMAs are heavily dependent on mechanisms that develop from the atomic scale.

Author: Ayoub Chahbari, S4437969
Group 20

1st Supervisor: Francesco Maresca, PhD
2nd Supervisor: G.H. Jonker, dr. ir.
Daily Supervisor: Lorenzo La Rosa, MSc

16th of June 2023

CONTENTS

I. Introduction

Upon applying an external stimulus (stress or temperature), Shape-memory alloys (SMA) can sustain large deformations, which are recovered after removing the external stimulus, due to internal microstructural changes that restore the original shape of the material [1]. SMAs, particularly Ni-Ti, have been crucial in engineering and industrial applications because of their ability to act as sensors and actuators [2], [3]. With the development of 'smart' systems, the increased use of actuators and sensors has become necessary, and the industry constantly needs better-performing sensors and actuators. Therefore, a thorough understanding of the Shape-Memory Effect (SME) has become crucial to designing better-performing SMAs.

Depending on the atomic composition and the annealing process, the rhombohedral (R) symmetry is a typical martensitic crystal structure in Ni-Ti at room temperature that arises upon a martensitic transformation (MT) from the cubic austenite [4]. The high symmetric structure of the austenite allows the nucleation of martensite variants of R crystals that can arrange into twinning systems [5]. Experiments showed that transformation twins are common in the SMAs martensitic microstructure [6]. However, these typical microstructures also arise in the Ge-Te system [7], which undergoes the same MT but is not an SMA.

Classical theories, such as the Energy Minimization Theory (EMT) [8], and the Phenomenological Theory of Martensite Crystallography (PTMC) [9], can predict the twinned microstructures of metallic compounds that undergo MTs (e.g., see [6], [10]). However, to the author's knowledge, despite having a similar microstructure, research has yet to be conducted to understand the difference between Ni-Ti and Ge-Te. Hence, this research aims to understand the difference between Ni-Ti and Ge-Te by thoroughly analysing their twinning systems.

II. Problem context

To understand the context and scope of the problem, a why-what model is used to delineate the main problem into its higher- and lower-order problems. As seen in Figure 1, the main problem is stated as follows: "*The cause of the SME is poorly/not understood*". This problem stems from the fact that there is a necessity for good-performing actuators and sensors. The main problem is of concern for a larger research program. However, the research proposed by this paper focuses only on a small part of the main problem. It follows from the main problem that no known analysis of the similarities and differences of the twinning systems in Ni-Ti and Ge-Te exists. This is seen in the lower part of the why-what model. By focusing on this lower-order problem, the boundary of this research is set on explaining the SME solely on the analysis of the twinning systems in Ni-Ti and Ge-Te.

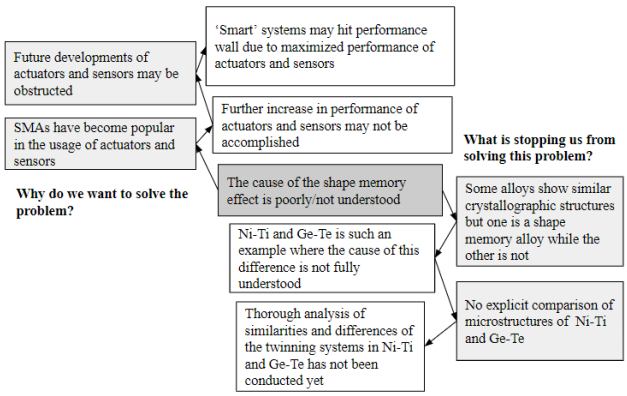

Fig. 1: Why-what analysis model - Analysis of the central issue by defining broader and narrower problems

III. Literature review

A. Industrial applications

SMAs play a crucial role in industrial applications. They are widely used for the following applications: aerospace, automotive, automation and control, appliance, energy, chemical processing, heating and ventilation, safety and security, and electronics industries [2]. In the automotive industry, the number of actuators and sensors have become increasingly important. such as stop-start systems, hybrid drivetrains and automated cruisecontrol. Similarly, SMAs are used in aerospace for shape morphing parts (such as wings) to improve the aerodynamic performance. SMAs are also essential for the human healthcare. Applications such as stents and human tissue, bone or tendon implants make use of SMAs (Ni-Ti). This is due to the fact that SMAs have pysical properties which can replicate human body parts. For an extensive review of industrial applications, see e.g. Jani, Leary, Subic, *et al.* [2]

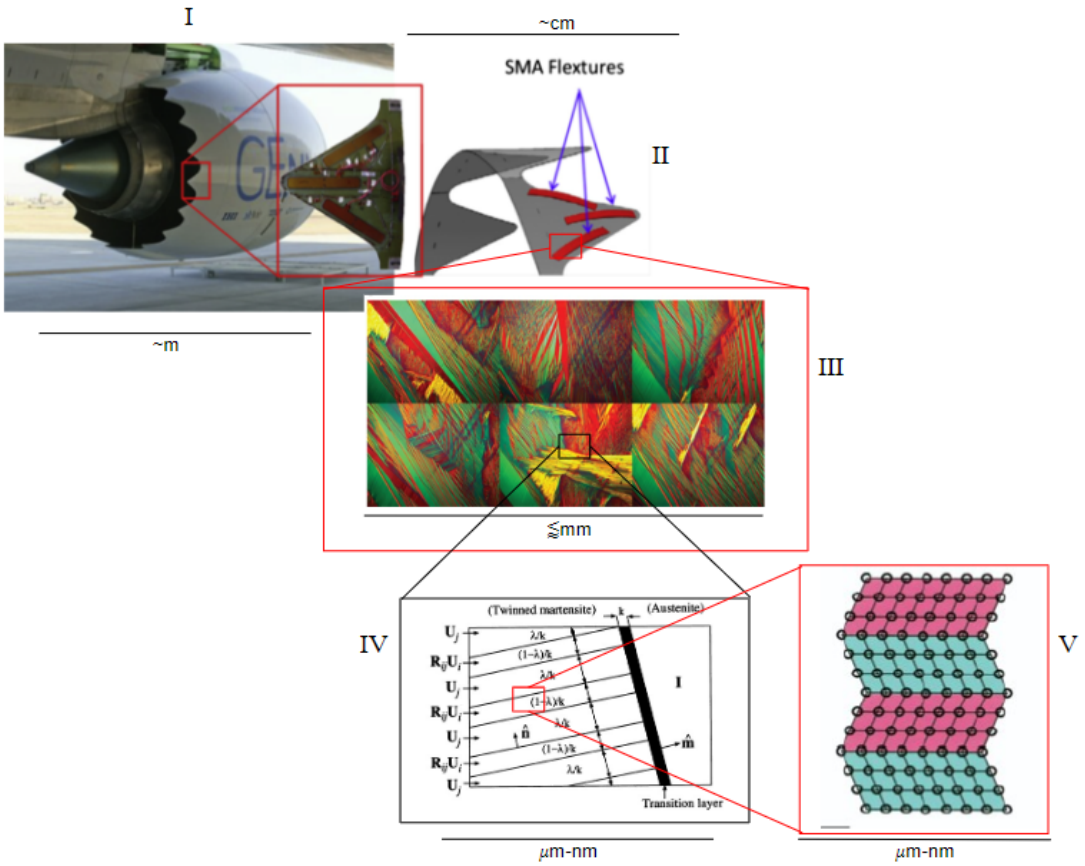

Fig. 2: Example of an application of SMAs in aerospace industry. The figure shows the material structure of the SMA at the macro- and microscale levels. Level 1 shows a jet engine cover, level 2 shows the SMA strips inside the material, level 3 shows micrographs of the MT from austenite to martensite, level 4 shows a schematic overview of the austenite and twinned martensite interface and level 5 shows a simplified representation of twinning in martensite [2], [3], [11], [12].

B. Material structure

As mentioned in section I, the SME occurs in the martensite phase of the SMA. To show the material structure of SMA, Figure 2 shows an example of an application in aerospace industry. If we zoom in, we can see the microstructure of the SMA. It is observed that the material shows an ordered structure. However, this is only true for the grains. It is also shown by Song, Chen, Dabade, *et al.* [11] that the microstructure of SMAs cannot be replicated, as this changes drastically upon repeating the MT from austenite to martensite. Despite this fact, we can still find a similar structure if we look at a smaller scale. Here, it is observed that the martensite forms a general ordered structure with a coherent interface with the austenite. This ordered structure is a twinning system.

C. Twinning systems

A twin is a planar crystal defect [13] whereby one side of the lattice can be obtained from the other by either a simple shear deformation or a rotation of the other lattice side [6]. Twinning occurs upon MTs in several metallic compounds [6], [9], [13]. Therefore, understanding the MT from cubic symmetric to rhombohedral lattices is necessary to understand twinning systems in Ni-Ti and Ge-Te. During MT, the austenite transforms into martensite that nucleates in the form of several variants. These so-called martensite variants have the same crystal structure but different space orientations [3], and they typically arrange into twinning systems, as illustrated in the level 5 sketch in Figure 2. During this process, the crystal does not tear apart/fracture, and experiments usually show continuity in the deformation at the twin interfaces [6]. When a twin arises upon MT, it is called a transformation twin. Mathematically, we can ensure such a continuity of the deformation (no fracture due to MT) at the twin interface with the *twinning equation*,

$$\mathbf{Q}\mathbf{U}_I - \mathbf{U}_J = \mathbf{a} \otimes \mathbf{n}, \tag{1}$$

where $\mathbf{a}$ is the shear vector, $\mathbf{n}$ is the twin plane, $\mathbf{Q}$ is a rotation tensor, and $\mathbf{U}_I$ and $\mathbf{U}_J$ are the Bain strain of the variants I and J, respectively. By solving Equation 1 (i.e. the twinning equation), it is possible to predict the twinning systems of an alloy that undergoes an MT, given its lattice parameters. Ball and James [8] showed how to obtain the general solutions of Equation 1, however, if a 180° rotation symmetry relates the twin variants I and J, then Mallard's law applies, and we can compute the vectors $\mathbf{a}$ and $\mathbf{n}$ as described by Bhattacharya and *et al.* [6]. Lastly, it is common to express the vectors $\mathbf{a}$ and $\mathbf{n}$ with respect the martensite lattice as

$$s = |\mathbf{a}||\mathbf{U}_J^{-1}\mathbf{n}|, \ \eta_1 = \frac{\mathbf{a}}{|\mathbf{a}|}, \ \mathbf{K}_1 = \frac{\mathbf{U}_J^{-1}\mathbf{n}}{|\mathbf{U}_J^{-1}\mathbf{n}|}, \tag{2}$$

where s is the twinning shear, η_1 is the shear direction and K_1 is the twin plane.

According to Bhattacharya and *et al.* [6] and Bilby and Crocker [14], twins can be classified into three different types being a *Type* 1, *Type* 2 or *Compound* twin. A *Type* 1 twin is where the twinning plane is a plane of symmetry in the austenite and thus having rational components. The *Type* 2 twin occurs when the shearing direction is a direction of symmetry in the austenite and hence rational. At last, *compound* twins are when a twin has both rational components for the twinning plane and shear direction.

D. Material properties

Lattice parameters are important for determining the twinning systems of metallic compounds because they are the only input needed to solve Equation 1. Experiments showed that lattice parameters may vary depending on temperature and the atomic concentration [15]. However, recently it has been shown that in Ni-Ti these dependencies are negligible [16]. Therefore this work will consider the average values of the lattice parameters. In the case of MT from the cubic austenite to the R martensitic phase, the matrices shown in Figure 3 represent the Bain strains of the transformation. It is important to note that Zhang and Sehitoglu [5], James and Hane [17] and Hane and Shield [12] assume the lengths of the cubic and rhombohedral lattices to be similar. Consequently, no explicit lattice lengths can be found for rhombohedral phases in literature such as seen in the paper by Vermeulen, Kumar, Brink, *et al.* [7]. Therefore, it is assumed that the rhombohedral lattice has the same lengths as the cubic lattice. The lattice lengths for Ni-Ti R-phase are $a_0 = 3.015\mathring{A}$ [16] and $a_0 = 5.97\mathring{A}$ for Ge-Te [7]

$$U_1 = \begin{pmatrix} \alpha & \delta & \delta \\ \delta & \alpha & \delta \\ \delta & \delta & \alpha \end{pmatrix} \qquad U_2 = \begin{pmatrix} \alpha & -\delta & -\delta \\ -\delta & \alpha & \delta \\ -\delta & \delta & \alpha \end{pmatrix}$$
$$U_3 = \begin{pmatrix} \alpha & \delta & -\delta \\ \delta & \alpha & -\delta \\ -\delta & -\delta & \alpha \end{pmatrix} \qquad U_4 = \begin{pmatrix} \alpha & -\delta & \delta \\ -\delta & \alpha & -\delta \\ \delta & -\delta & \alpha \end{pmatrix}$$

Fig. 3: Transformation matrices for the different number of martensite variants [6]

The α and δ parameters, introduced in the Bain Strains in Figure 3, are defined by the following relations,

$$\alpha = \frac{\sqrt{1+2cos(\gamma)} + 2\sqrt{1-cos(\gamma)}}{3}, \tag{3}$$

$$\delta = \frac{\sqrt{1+2cos(\gamma)} - \sqrt{1-cos(\gamma)}}{3}, \tag{4}$$

where γ is the angle of the rhombohedral lattice. This angle is $\gamma \approx 88.20°$ for Ge-Te [7] and $\gamma \approx 89.5°$ for Ni-Ti R phase [18].

IV. Conceptual Research Design

A. Problem statement

Based on the literature review (section III) and the problem context (section II), the following problem statement has been formulated:

"*Ni-Ti and Ge-Te have the same microstructure, although they differ as only Ni-Ti shows the SME. However, it is currently not well understood why Ni-Ti and Ge-Te show this difference due to poor knowledge of the cause of the SME. This prevents future developments of SMAs.*"

B. Research objective

Using theory on setting SMART goals from Bjerke and Renger [19] and Verschuren, Doorewaard, and Mellion [20], the following research objective is formulated:

"*The objective of this research is to thoroughly analyse the similarities and differences of the twinning systems in Ni-Ti and Ge-Te using analytical methods described in section III and computational methods. The analysis will be used to explain what causes the SME*"

C. Research framework

Based on the problem context (section II), literature review (section III), and the research objective (subsection IV-B), a framework has been constructed. From the framework, it is clear what information needs to be gathered to select relevant assessment criteria for validating the deliverable.

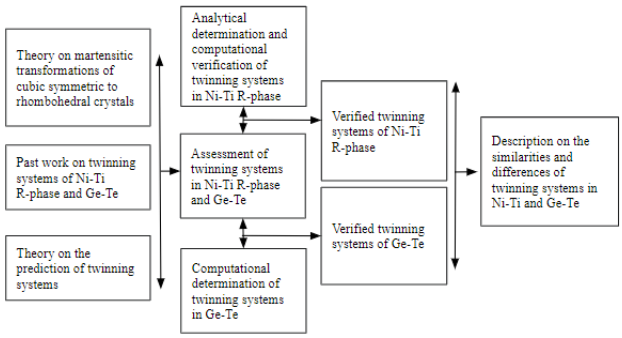

Fig. 4: Research framework - Schematic representation of the steps needed to achieve the objective

D. Research questions

To carry out research that can provide the necessary knowledge on the cause of the SME described in subsection IV-B and outlined in the research framework (Figure 4), a set of research questions has been formulated:

"*What is the cause of the SME in metallic compounds based on analysing the twinning systems in Ni-Ti and Ge-Te?*"

The central research question has been divided into three sub-questions that aim to answer the central question and provide a steering function for the research design in further sections.

1) *What twinning systems can be found in Ni-Ti R-phase?*
2) *How to computationally verify twinning systems in rhombohedral crystal structures?*
3) *What twinning systems can be found in martensite Ge-Te?*

V. Technical research design

The following section discusses the methods and validation necessary to obtain knowledge to answer the research questions stated in subsection IV-D.

A. Research materials

To start the proposed research, it is necessary to consider the research methods that provide an answer to each of the sub-questions (subsection IV-D). Using both the recommendations of the supervisors and the methods discussed in the papers by Zhang and Sehitoglu [5] and Vermeulen, Kumar, Brink, *et al.* [7] and the book by Bhattacharya and *et al.* [6], the methods discussed below are considered.

The first sub-question will be answered using analytical methods explained in subsection III-C. The twinning equation explained in this section will be used together with the lattice parameters defined in subsection III-D, used for the Bain matrices. These will be combined with Mallard's law to find the twinning systems of the Ni-Ti R-phase.

Due to prior experience with this programming language and the supervisor's recommendation, the computational code will be designed using Matlab. The procedure for finding the twinning systems in Ni-Ti R-phase will be translated into a computational script/function.

The last sub-question will be answered using the developed code. Using the lattice parameters of Ge-Te, the code will give the corresponding twinning systems. This is then compared with the twinning systems in Ni-Ti, where the differences and similarities are analysed.

B. Validation of found twinning systems

After defining the methods to answer the research question, the result must be validated. The results for the first sub-question will be validated using the paper by Zhang and Sehitoglu [5] together with other papers on the twinning systems of Ni-Ti. The Matlab code is validated by comparing its result with the results of sub-question 1. Last, the twinning equations obtained for Ge-Te are verified using the paper by Vermeulen, Kumar, Brink, *et al.* [7] along with other papers on the twinning systems of Ge-Te.

C. Research procedure

The following section will describe the key steps necessary for the analysis of the twinning systems in Ni-Ti and Ge-Te. Crystallographic theories introduced in section III will be further described in terms of its applications. Below, an overview of the procedure is given after which an explanation of each step will be given.

1) Find all 24 rotation matrices of the austenite point group

2) Use each π-rotation in the austenite point group to generate new Bain matrices
3) Use the rotation axis, around which the π-rotation is defined, to solve the twinning equation
4) Verify the stability of the found twin using the habit plane equation

1) Point group group rotations: As explained in section I, twinning occurs upon the MT from cubic austenite. This transformation is represented in the form of the Bain strain matrices (Figure 3). These matrices transform austenite in four different variants that are related through the point group rotations [5], [6], [12]. As shown in Equation 5, the point group rotation is represented by $\mathbf{R}$ and the Bain strain matrix by $\mathbf{U}$. A point group is a set of rotations/reflections that do not alter the crystal structure. The point group of a cubic crystal consists of a group of 24 rotations [6].

$$\mathbf{U}_I = \mathbf{R}^T \mathbf{U}_J \mathbf{R} \tag{5}$$

The first step is to find all 24 rotation matrices of the austenite point group. This is necessary since these rotations determine how variants form pairs in order to form a twin. The rotation matrices describe not only to what degree the lattice is rotated but also with respect to what axis. This axis ($\hat{e}$) is essential for finding the twinning systems since there is a dependency for both the twin plane ($\mathbf{n}$) and twin direction ($\mathbf{a}$).

2) Martensite variant pairs: The next step is to identify how martensite variants will form pairs to establish a twin. This is done by using Equation 5 which describes how the variants are related through rotations. We know the interface of the formed pair by applying this equation with respect to one of the variants and using all 24 π-rotations. This result will be used for the next step solving the twinning equation.

3) Solving the twinning equation: The third step is to solve the twinning equation. We are able to solve the twinning equation using Mallard's law under the condition the variants form a pair through a 180° rotation about some axis $\hat{e}$ [6]. Once the 180° rotations are verified in the previous step, Mallard's law states two solutions to the twinning equation (1) being the following:

$$\mathbf{a}_1 = 2\left(\frac{\mathbf{U}_J^{-1}\cdot\hat{e}}{|\mathbf{U}_J^{-1}\cdot\hat{e}|} - \mathbf{U}_J\cdot\hat{e}\right) \text{ and } \mathbf{n}_1 = \hat{e} \tag{6}$$

$$\mathbf{a}_2 = \rho\mathbf{U}_J\cdot\hat{e} \text{ and } \mathbf{n}_2 = \frac{2}{\rho}\left(\mathbf{I} - \frac{\mathbf{U}_J^T\cdot\mathbf{U}_J}{|\mathbf{U}_J\cdot\hat{e}|^2}\right)\cdot\hat{e} \tag{7}$$

where $\rho \neq 0$ is such that $|\mathbf{n}| = 1$ [5], [6], [16], [12]. The found twin/shear direction $\mathbf{a}$ and the twin plane $\mathbf{n}$ are with respect to the austenite basis. The vectors $\mathbf{a}$ and $\mathbf{n}$ can be transformed to the martensite basis using Equation 2 which is the customary way to express the solutions. According to the classification in subsection III-C, the solution to Equation 6 is called a *Type* 1 twin and the *Type* 2 twin is described by Equation 7.

4) Verify Austenite-Martensite coherency: The last step is to verify the Austenite-Martensite interface coherency, since the deformations must be continuous. To verify the compatibility, we will make use of the habit plane equation found in [6], [16], [12]. This equation predicts the interface, or habit plane, of the austenite-martensite interface. A coherent interface must be formed to ensure continuous deformation. It has been proven by Ball and James [8] that the habit plane equation has solutions if and only if the following two conditions are met:

$$\omega = \mathbf{a}\cdot\mathbf{U}_J\cdot(\mathbf{U}_J^2 - \mathbf{I})^{-1}\cdot\mathbf{n} \leq -2 \tag{8}$$

$$\psi = tr(\mathbf{U}_J^2) - det(\mathbf{U}_J^2) - 2 + \frac{|\mathbf{a}|^2}{2\omega} \geq 0 \tag{9}$$

If both Equation 8 and Equation 9 are satisfied, the coherency of the austenite-martensite interface is verified.

VI. Twinning systems in Ni-Ti and Ge-Te

A. Martensite variant pairs

The point group of the cubic austenite and the variant pairs are shown in Table I. The first column shows all rotations using the index notation. The rotations are ordered based on their respective angles. These rotation matrices are used in Equation 5 together with the variants shown in Figure 3 to find the correct twin pair. These pairs are represented in the remaining columns of the table below. For example, row 2 shows that the first variant ($\mathbf{U}_1$) transforms into the third variant ($\mathbf{U}_3$) using Equation 5. This means that these variants form a pair through the rotation and axis $\mathbf{R}[\hat{e}_1,90°]$. Consequently, the remaining variants form pairs with their respective rotations and axes. It is shown that all 12 pairs are formed through 180° rotations. This has also been shown by Zhang and Sehitoglu [5] and Hane and Shield [12]. Therefore, we have verified that Mallard's law can be used to find all possible twins.

TABLE I: Symmetry transformations between the variants. The first column lists all the cubic Laue group rotations. The remaining columns show the relation between the variants based on the Laue group rotation.

Rotation	$\mathbf{U}_1$	$\mathbf{U}_2$	$\mathbf{U}_3$	$\mathbf{U}_4$
$\mathbf{I} = \hat{e}_1 \otimes \hat{e}_1 + \hat{e}_2 \otimes \hat{e}_2 + \hat{e}_3 \otimes \hat{e}_3$	1	2	3	4
$\mathbf{R}[\hat{e}_1, 90^\circ] = \hat{e}_1 \otimes \hat{e}_1 - \hat{e}_2 \otimes \hat{e}_3 + \hat{e}_3 \otimes \hat{e}_2$	3	4	2	1
$\mathbf{R}[\hat{e}_2, 90^\circ] = \hat{e}_1 \otimes \hat{e}_3 + \hat{e}_2 \otimes \hat{e}_2 + \hat{e}_3 \otimes \hat{e}_1$	2	4	1	3
$\mathbf{R}[\hat{e}_3, 90^\circ] = -\hat{e}_1 \otimes \hat{e}_2 + \hat{e}_2 \otimes \hat{e}_1 + \hat{e}_3 \otimes \hat{e}_3$	4	1	2	3
$\mathbf{R}[\hat{e}_1 + \hat{e}_2 + \hat{e}_3, 120^\circ] = \hat{e}_1 \otimes \hat{e}_3 + \hat{e}_2 \otimes \hat{e}_1 + \hat{e}_3 \otimes \hat{e}_2$	1	3	4	2
$\mathbf{R}[\hat{e}_1 + \hat{e}_2 - \hat{e}_3, 120^\circ] = \hat{e}_1 \otimes \hat{e}_2 - \hat{e}_2 \otimes \hat{e}_3 - \hat{e}_3 \otimes \hat{e}_1$	4	1	3	2
$\mathbf{R}[\hat{e}_1 - \hat{e}_2 + \hat{e}_3, 120^\circ] = -\hat{e}_1 \otimes \hat{e}_2 - \hat{e}_2 \otimes \hat{e}_3 + \hat{e}_3 \otimes \hat{e}_1$	2	3	1	4
$\mathbf{R}[-\hat{e}_1 + \hat{e}_2 + \hat{e}_3, 120^\circ] = -\hat{e}_1 \otimes \hat{e}_2 + \hat{e}_2 \otimes \hat{e}_3 - \hat{e}_3 \otimes \hat{e}_1$	3	2	4	1
$\mathbf{R}[\hat{e}_1, 180^\circ] = \hat{e}_1 \otimes \hat{e}_1 - \hat{e}_2 \otimes \hat{e}_2 - \hat{e}_3 \otimes \hat{e}_3$	2	1	4	3
$\mathbf{R}[\hat{e}_2, 180^\circ] = -\hat{e}_1 \otimes \hat{e}_1 + \hat{e}_2 \otimes \hat{e}_2 - \hat{e}_3 \otimes \hat{e}_3$	4	3	2	1
$\mathbf{R}[\hat{e}_3, 180^\circ] = -\hat{e}_1 \otimes \hat{e}_1 - \hat{e}_2 \otimes \hat{e}_2 + \hat{e}_3 \otimes \hat{e}_3$	3	4	1	2
$\mathbf{R}[\hat{e}_1 + \hat{e}_2, 180^\circ] = \hat{e}_1 \otimes \hat{e}_2 + \hat{e}_2 \otimes \hat{e}_1 - \hat{e}_3 \otimes \hat{e}_3$	3	2	1	4
$\mathbf{R}[\hat{e}_1 - \hat{e}_2, 180^\circ] = -\hat{e}_1 \otimes \hat{e}_2 - \hat{e}_2 \otimes \hat{e}_1 - \hat{e}_3 \otimes \hat{e}_3$	1	4	3	2
$\mathbf{R}[\hat{e}_2 + \hat{e}_3, 180^\circ] = -\hat{e}_1 \otimes \hat{e}_1 + \hat{e}_2 \otimes \hat{e}_3 + \hat{e}_3 \otimes \hat{e}_2$	2	1	3	4
$\mathbf{R}[\hat{e}_2 - \hat{e}_3, 180^\circ] = -\hat{e}_1 \otimes \hat{e}_1 - \hat{e}_2 \otimes \hat{e}_3 - \hat{e}_3 \otimes \hat{e}_2$	1	2	4	3
$\mathbf{R}[\hat{e}_1 + \hat{e}_3, 180^\circ] = \hat{e}_1 \otimes \hat{e}_3 - \hat{e}_2 \otimes \hat{e}_2 + \hat{e}_3 \otimes \hat{e}_1$	4	2	3	1
$\mathbf{R}[\hat{e}_1 - \hat{e}_3, 180^\circ] = -\hat{e}_1 \otimes \hat{e}_3 - \hat{e}_2 \otimes \hat{e}_2 - \hat{e}_3 \otimes \hat{e}_1$	1	3	2	4
$\mathbf{R}[\hat{e}_1 + \hat{e}_2 + \hat{e}_3, 240^\circ] = \hat{e}_1 \otimes \hat{e}_2 + \hat{e}_2 \otimes \hat{e}_3 + \hat{e}_3 \otimes \hat{e}_1$	1	4	2	3
$\mathbf{R}[\hat{e}_1 + \hat{e}_2 - \hat{e}_3, 240^\circ] = -\hat{e}_1 \otimes \hat{e}_3 + \hat{e}_2 \otimes \hat{e}_1 - \hat{e}_3 \otimes \hat{e}_2$	2	4	3	1
$\mathbf{R}[\hat{e}_1 - \hat{e}_2 + \hat{e}_3, 240^\circ] = \hat{e}_1 \otimes \hat{e}_3 - \hat{e}_2 \otimes \hat{e}_1 - \hat{e}_3 \otimes \hat{e}_2$	3	1	2	4
$\mathbf{R}[-\hat{e}_1 + \hat{e}_2 + \hat{e}_3, 240^\circ] = -\hat{e}_1 \otimes \hat{e}_3 - \hat{e}_2 \otimes \hat{e}_1 + \hat{e}_3 \otimes \hat{e}_2$	4	2	1	3
$\mathbf{R}[\hat{e}_1, 270^\circ] = \hat{e}_1 \otimes \hat{e}_1 + \hat{e}_2 \otimes \hat{e}_3 - \hat{e}_3 \otimes \hat{e}_2$	4	3	1	2
$\mathbf{R}[\hat{e}_2, 270^\circ] = -\hat{e}_1 \otimes \hat{e}_3 + \hat{e}_2 \otimes \hat{e}_2 + \hat{e}_3 \otimes \hat{e}_1$	3	1	4	2
$\mathbf{R}[\hat{e}_3, 270^\circ] = \hat{e}_1 \otimes \hat{e}_2 - \hat{e}_2 \otimes \hat{e}_1 + \hat{e}_3 \otimes \hat{e}_3$	2	3	4	1

B. Twinning in martensite

In the MT from cubic (austenite) to rhombohedral (martensite) the lattice lengths between both phases are similar as stated in subsection III-D. Therefore, the Bain matrices only have a dependency on the lattice angle (γ) as shown in Equation 3 and 4. Accordingly, Equation 6 and 7 will be a function of only one lattice parameter, the lattice angle γ. This allows us to express the twin plane and the shear direction as a function of γ. Accordingly, we can obtain a general solution for the twinning systems for MT from cubic (austenite) to rhombohedral (martensite) systems.

$$\mathbf{a}_1 = \frac{2\delta(2\alpha+\delta)}{2\delta^2+(\alpha+\delta)^2}\begin{pmatrix}2\delta\\ \alpha+\delta\\ \alpha+\delta\end{pmatrix} \text{ and } \mathbf{n}_1 = \begin{pmatrix}1\\0\\0\end{pmatrix} \quad (10)$$

$$\mathbf{a}_2 = 2\sqrt{2}\frac{\delta^2+2\alpha\delta}{\alpha^2+2\delta^2}\begin{pmatrix}\alpha\\ \delta\\ \delta\end{pmatrix} \text{ and } \mathbf{n}_2 = \begin{pmatrix}0\\1\\1\end{pmatrix} \quad (11)$$

Equation 10 and 11 show the solution for the shear direction and twin plane for the variant pair $\mathbf{U}_1$ and $\mathbf{U}_2$. Here α and δ are similarly defined as in Equation 3 and 4. Notice that only the shear directions have a dependency on the lattice angle. Repeating the process for the remaining 11 variant pairs, we obtain the general twinning systems for MT from cubic (austenite) to rhombohedral (martensite). The general twinning systems have been summarized in Table II where τ and ρ are defined as $\frac{2\delta(2\alpha+\delta)}{2\delta^2+(\alpha+\delta)^2}$ and $2\sqrt{2}\frac{\delta^2+2\alpha\delta}{\alpha^2+2\delta^2}$, respectively. These generalized solutions have also been found by Hane and Shield [12], [21] and James and Hane [17] verifying the summarized results in Table II.

TABLE II: General solution for the twinning systems in materials transforming from cubic to rhombohedral with respect to the cubic basis.

Pair	$\mathbf{n}_1$	$\mathbf{a}_1$	$\mathbf{n}_2$	$\mathbf{a}_2$
$\mathbf{U}_1$ to $\mathbf{U}_2$	(1,0,0)	$\tau[2\delta, \alpha+\delta, \alpha+\delta]$	(0,1,1)	$\rho[\alpha, \delta, \delta]$
$\mathbf{U}_2$ to $\mathbf{U}_1$	(1,0,0)	$\tau[-2\delta, \alpha+\delta, \alpha+\delta]$	(0,1,1)	$\rho[-\alpha, \delta, \delta]$
$\mathbf{U}_1$ to $\mathbf{U}_3$	(0,0,1)	$\tau[\alpha+\delta, \alpha+\delta, 2\delta]$	(1,1,0)	$\rho[\delta, \delta, \alpha]$
$\mathbf{U}_3$ to $\mathbf{U}_1$	(0,0,1)	$\tau[\alpha+\delta, \alpha+\delta, -2\delta]$	(1,1,0)	$\rho[\delta, \delta, -\alpha]$
$\mathbf{U}_1$ to $\mathbf{U}_4$	(0,1,0)	$\tau[\alpha+\delta, 2\delta, \alpha+\delta]$	(1,0,1)	$\rho[\delta, \alpha, \delta]$
$\mathbf{U}_4$ to $\mathbf{U}_1$	(0,1,0)	$\tau[\alpha+\delta, -2\delta, \alpha+\delta]$	(1,0,1)	$\rho[\delta, -\alpha, \delta]$
$\mathbf{U}_2$ to $\mathbf{U}_3$	(0,1,0)	$\tau[-(\alpha+\delta), 2\delta, \alpha+\delta]$	(1,0,-1)	$\rho[-\delta, \alpha, \delta]$
$\mathbf{U}_3$ to $\mathbf{U}_2$	(0,1,0)	$\tau[\alpha+\delta, 2\delta, -(\alpha+\delta)]$	(1,0,-1)	$\rho[\delta, \alpha, -\delta]$
$\mathbf{U}_2$ to $\mathbf{U}_4$	(0,0,1)	$\tau[-(\alpha+\delta), \alpha+\delta, 2\delta]$	(1,-1,0)	$\rho[-\delta, \delta, \alpha]$
$\mathbf{U}_4$ to $\mathbf{U}_2$	(0,0,1)	$\tau[\alpha+\delta, -(\alpha+\delta), 2\delta]$	(1,-1,0)	$\rho[\delta, -\delta, \alpha]$
$\mathbf{U}_3$ to $\mathbf{U}_4$	(1,0,0)	$\tau[2\delta, \alpha+\delta, -(\alpha+\delta)]$	(0,1,-1)	$\rho[\alpha, \delta, -\delta]$
$\mathbf{U}_4$ to $\mathbf{U}_3$	(1,0,0)	$\tau[2\delta, -(\alpha+\delta), \alpha+\delta]$	(0,1,-1)	$\rho[\alpha, -\delta, \delta]$

The next step is to transform the generalized results to the rhombohedral basis. This is done numerically due to the complexity of the problem. The first step is to find the rotation matrix $\mathbf{Q}$ seen in the twinning equation (1). We have to invert the $\mathbf{Q}$ rotation to obtain the twinning equation with respect to the martensite basis. The rotation matrix $\mathbf{Q}$ is defined by the polar decomposition theorem,

$$\mathbf{F} = \mathbf{Q} \cdot \mathbf{B} \quad (12)$$

Where $\mathbf{F}$ is the deformation gradient describing the direct transformation of the austenite to the martensite phase, and $\mathbf{B}$ the bain strain matrix. Since both $\mathbf{F}$ and $\mathbf{B}$ are known, the rotation matrix $\mathbf{Q}$ can be determined by rewriting Equation 12 in terms of $\mathbf{Q}$.

TABLE III: Computationally determined twinning systems and lattice shear in Ni-Ti R-phase and Ge-Te with respect to the martensite basis. The left and right values for shear represent Ni-Ti and Ge-Te, respectively.

Twinning pair	η_1	κ_1	η_2	κ_2	Shear
"1-2"	(0,1,1)	[1,0,0]	(1,0,0)	[0,1,1]	[0.024577][0.087564]
"2-1"	(0,1,1)	[1,0,0]	(1,0,0)	[0,1,1]	[0.024577][0.087564]
"1-3"	(1,1,0)	[0,0,1]	(0,0,1)	[1,1,0]	[0.024577][0.087564]
"3-1"	(1,1,0)	[0,0,1]	(0,0,1)	[1,1,0]	[0.024577][0.087564]
"1-4"	(1,0,1)	[0,1,0]	(0,1,0)	[1,0,1]	[0.024577][0.087564]
"4-1"	(1,0,1)	[0,1,0]	(0,1,0)	[1,0,1]	[0.024577][0.087564]
"2-3"	(1,0,-1)	[0,1,0]	(0,1,0)	[1,0,-1]	[0.024577][0.087564]
"3-2"	(1,0,-1)	[0,1,0]	(0,1,0)	[1,0,-1]	[0.024577][0.087564]
"2-4"	(1,-1,0)	[0,0,1]	(0,0,1)	[1,-1,0]	[0.024577][0.087564]
"4-2"	(1,-1,0)	[0,0,1]	(0,0,1)	[1,-1,0]	[0.024577][0.087564]
"3-4"	(0,1,-1)	[1,0,0]	(1,0,0)	[0,1,-1]	[0.024577][0.087564]
"4-3"	(0,1,-1)	[1,0,0]	(1,0,0)	[0,1,-1]	[0.024577][0.087564]

Subsequently, Equation 2 is used to compute the twins with respect to the martensite basis. These results are shown in Table III. Despite having different lattice parameters, both Ni-Ti R-phase and Ge-Te showed similar results for the twinning equation with respect to the martensite basis. In Table III, it is seen that both alloys form a rational twinning plane and direction. Therefore, the only possible solutions to the twinning equation are he compound twins $\{100\}\langle 110\rangle$ and $\{110\}\langle 100\rangle$. This has been compared with existing literature which confirmed our results [5], [7], [17], [12], [22], [23].

A significant difference is observed when comparing the shear of Ni-Ti and Ge-Te. Despite the small difference in lattice angle of approximately 1.3°, the shear of Ge-Te is approximately 3.5 times higher. To explain this significant difference, we must express the shear with respect to the lattice angle. Using the shear defined in Equation 2, the following shear lattice angle relation is derived.

$$s = \frac{2\sqrt{2}|\cos(\gamma)|}{\sqrt{1+\cos(\gamma)-2\cos^2(\gamma)}} \tag{13}$$

In Equation 13, it is observed that shear follows an inverse square root relation with respect to the lattice angle. This translates to a nonlinear relationship where a decreasing lattice angle leads to an increase in shear. This behaviour is visualised in Figure 5 where shear is plotted against the lattice angle in the range of 87 and 93 degrees. Experiments have shown that the lattice angle of the R-phase lies within this range [5], [7]. In Figure 5 it is seen that the slope of the curve is high. This insinuates that the lattice shear is sensitive for small changes in the lattice angle (γ).

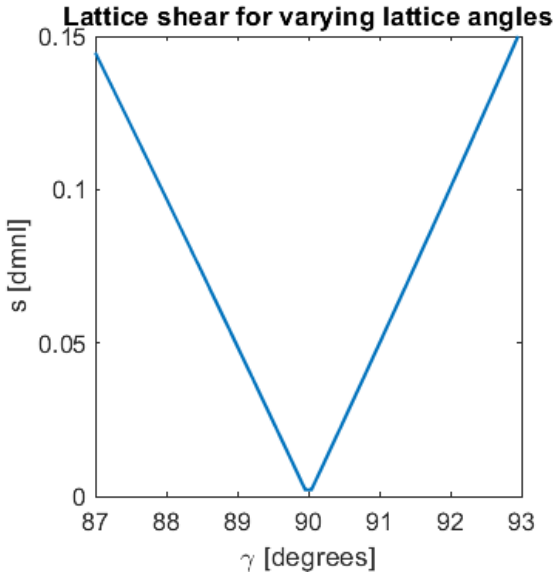

Fig. 5: A range of lattice shear computed against the lattice angle as shown in Equation 13

C. Austenite-Martensite coherency

The last step is to validate the coherency of the interface between the twinning systems $\{100\}$ and $\{110\}$ and the austenite. Upon quenching of the austenite phase, coexistence of the twinned martensite and the austenite will occur as shown in Figure 6. An important property of the transition between austenite and twinned martensite is coherency. Without coherency, the material will fracture making the above results invalid since these assume continuous deformation.

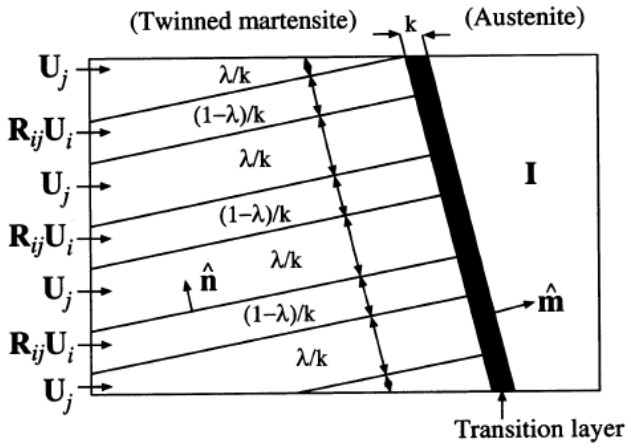

Fig. 6: Schematic of the austenite and twinned martensite upon quenching found in Figure 2 [12]

Again, we can express both Equation 8 and 9 in terms of the lattice angle. This allows a generalization for the MT from cubic to rhombohedral. Since we showed that only the $\{100\}$ and $\{110\}$ twins will form, two conditions can be obtained as shown below [12],

$$\omega_{\{100\}} = -sec^2(\frac{\gamma}{2}), \psi_{\{100\}} = cos^2(\gamma)(1-2cos(\gamma)) \tag{14}$$

$$\omega_{\{110\}} = -2,\ \psi_{\{110\}} = \psi_{\{100\}} = \psi \tag{15}$$

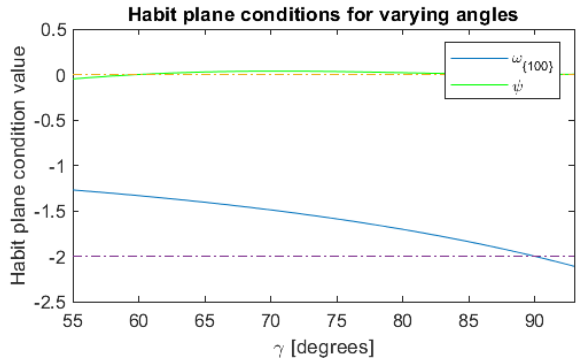

Fig. 7: Plot of $\omega_{\{100\}}$ and ψ against the lattice angle

The functions ω and ψ of Equation 14 and 15 are found for the $\{100\}$ and $\{110\}$ twins, respectively. It can be observed that the second condition ψ does not depend on the twin plane since for both Equation 14 and 15 the same ψ was found. However, the first condition does show a dependency on the twin plane. As seen in Equation 15, the first condition is exactly -2, thus satisfying Equation 8. Figure 7 shows $\omega_{\{100\}}$ and ψ against the lattice angle. It is seen that the habit plane condition will only be met for $\omega_{\{100\}}$ if $\gamma \geq 90°$ and for ψ if $\gamma \geq 60°$. Since the lattice angle of both Ni-Ti and Ge-Te are below 90°, the habit plane conditions are not satisfied for the twinning systems $\{100\}$. Instead, the second condition is satisfied since the lattice angle of both Ni-Ti and Ge-Te are greater than 60°.

D. Main findings

Using the twinning equation and Mallards' law, it is shown that a generalised twinning system can be derived for MT from cubic to rhombohedral. Upon transforming the results obtained from Mallard's law to the martensite basis, it is found that both Ni-Ti R-phase and Ge-Te form the same $\{100\}\langle 110\rangle$ and $\{110\}\langle 100\rangle$ compound twins. However, a significant difference is seen in the lattice shear. Using the habit plane condition, it is shown that only the $\{110\}$ can be a lattice invariant shear for the transformation and thus the only possible transformation twin. However, experiments show that the $\{100\}$ does exist in the martensite microstructure [5], [7], as a deformation twin.

From our results, there is no clear distinction between the twinning systems in Ni-Ti and Ge-Te, except for the twinning shear magnitude. The latter might induce plasticity and hence hinder the SME. Yet, EMT is not sufficient to explain why Ni-Ti shows the SME while Ge-Te does not. The reason resides in the fact that the solutions of the crystallographic theories depend only on the point group of a crystal and on the lattice parameters, neglecting the atomic arrangements inside the crystal cells. Consequently, a thorough analysis of both alloys is needed to show any differences in the crystal structures.

VII. Crystallography of Ni-Ti and Ge-Te

A. Crystallographic hierarchy

Crystal structures are classified according to space groups. Space groups are a set of symmetry elements and operations, which completely describe the spatial arrangement of a 3D periodic pattern [24]. Therefore, the space group of a crystal is a short-hand notation that combines the information about the Bravais lattice and point group of that crystal (Table IV). All crystal structures can be described using 230 space groups.

TABLE IV: The 32 point groups, 14 Bravais lattices, lattice parameters and their respective crystal system. The bold point groups are the general expression for the crystal systems. P represents a primitive cell, I represents a body centered cell, S represents a base centered cell, R represents a rhombohedral and F represents a face centered cell. For the Trigonal system, only the lattice parameters of the rhombohedral lattice are given since the hexagonal lattice parameters are already defined the row above.

Crystal system	Point group	Bravais lattice	lattice parameters
Triclinic	1, $\bar{\mathbf{1}}$	Triclinic (P)	$a \neq b \neq c$ $\alpha \neq \beta \neq \gamma$
Monoclinic	2, m, **2/m**	Monoclinic (P)(I)	$a \neq b \neq c$ $\alpha \neq 90°, \beta \neq \gamma$
Orthorombic	222, mm2, **mmm**	Orthorombic (P)(I)(S)(F)	$a \neq b \neq c$ $\alpha = \beta = \gamma = 90°$
Tetragonal	4, $\bar{4}$, 422, $\bar{4}$2m, 4/m, 4mm, **4/mmm**	Tetragonal (P)(I)	$a = b \neq c$ $\alpha = \beta = \gamma = 90°$
Hexagonal	6, $\bar{6}$, 622, $\bar{6}$2m, 6/m, 6mm, **6/mmm**	Hexagonal (P)	$a = b \neq c$ $\alpha = 120°, \beta = \gamma = 90°$
Trigonal	3, $\bar{3}$, 3m, 32, $\bar{\mathbf{3}}$**m**	Hexagonal (P), Rhombohedral (R)	$a = b = c$ $\alpha = \beta = \gamma \leq 120°$
Cubic	23, m$\bar{3}$, 432, $\bar{4}$3m, **m$\bar{3}$m**	Cubic (P)(I)(F)	$a = b = c$ $\alpha = \beta = \gamma = 90°$

In crystallography, crystals are periodic arrangements of atoms (i.e. lattice) and they can be represented by a lattice point. A Bravais lattice is defined as a lattice where the lattice points coincide after translating the crystal by one lattice unit [25]. In nature, it has been shown that only 14 Bravais lattices can be found, as summarized in Table IV. Differently, a point group is a set of symmetries which is invariant around a center point. These symmetry operations are composed of mirror planes, rotation axes and rotoinversion axes [26], [27]. Point groups are classified based on the number of symmetries. Based on this definition, only 32 possible point groups can be defined and appointed to their crystal system as seen in Table IV. As seen in this table, seven crystal systems are defined. However, crystal systems are a different concept from Bravais lattices. In fact, there are 7 crystal systems while there exist 14 Bravais lattices [26]. So, a crystal system can describe several Bravais lattices but the opposite does not apply. Figure 8 shows a schematic overview of the crystal classifications and how they are related to EMT

Knowing the space group of a crystal, the Wyckoff positions can be specified. Wyckoff positions use the symmetries of a crystal unit cell to specify the atomic arrangement. For example, the space group R3m has Bravais lattice R (rhombohedral) and space group 3m (3-fold rotation symmetry and 1 mirror plane). The Wyckoff positions for this space group are 3a, 9b and 18c. The number indicates the multiplicity of points within the unit cell and combined with the letter specifies the positions. Wyckoff position 3a imply that the atom positions are (0 0 z), (2/3 1/3 z+1/3) and (1/3 2/3 z+2/3) [24], [28], [29], [30], [31].

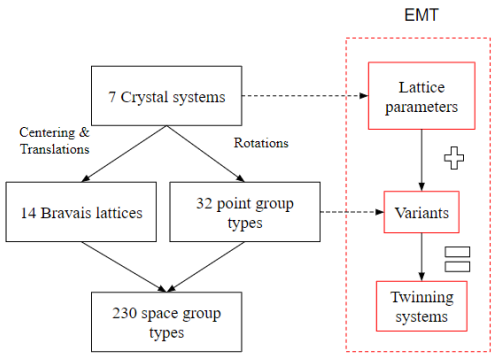

Fig. 8: Schematic overview of the crystallographic hierarchy

B. Trigonal systems

In literature, both Ni-Ti R-phase and Ge-Te are considered to have a rhombohedral lattice [5], [7], [17], [12], [22] and [23]. Therefore, both materials can be described with a trigonal crystal system. However, upon studying the crystallography it was found that a trigonal crystal system does not necessarily imply a material to be rhombohedral. As reported by Nespolo, Aroyo, and Souvignier [26], the trigonal crystal system can be described by both a hexagonal and rhombohedral Bravais lattices. Although having similar point groups, they are related to different space groups, thus implying a different arrangement of atoms within the trigonal cell. The hexagonal Bravais lattice is represented by the P in the space group notation while rhombehedral is represented by the R. A significant difference is that the

R Bravais lattice can be expressed by a non-primitive (conventional) hexagonal cell (Figure 9). Yet, this is not the case for the P Bravais lattice that can only be expressed only by a hexagonal cell.

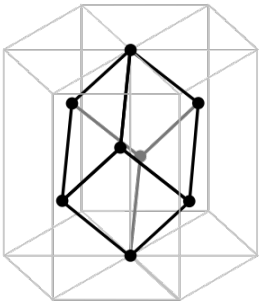

Fig. 9: Schematic overview of the relation between hexagonal and rhombohedral lattice.

C. Crystallography of Ge-Te

In the literature, Ge-Te with a trigonal system is reported to have the space group R3m, implying the P Bravais lattice and point group 3m [7], [32], [33]. According to the theory of subsection VII-A and VII-B, we validate that both the point and space group belong to the trigonal system. Furthermore, Ge-Te can either be expressed by a non-primitive hexagonal or rhombohedral cell.

To observe the crystal structure of Ge-Te and to validate the second statement, this research makes use of the OVITO software to visualize the crystal structure [34]. The data on the crystallography is obtained from the open databases *Materials Project* (MP) and *Crystallography open database* (COD) [33], [35]. Important to note that the crystallography data represents trigonal crystal systems using a hexagonal description. To show that Ge-Te is rhombohedral, we have to obtain the rhombohedral Bravais lattice from the hexagonal description as shown in Figure 9. Prior to visualizing the crystallography of Ge-Te, the Wyckoff positions reported by the open databases are compared to the general Wyckoff positions belonging to the R3m space group. Ge-Te is stated to have Wyckoff position 3a for both Ge and Te with positions (2/3 1/3 0.325557) and (1/3 2/3 0.195443), respectively [32], [33]. These positions comply with the general positions (0 0 z), (2/3 1/3 z+1/3) and (1/3 2/3 z+2/3). Therefore, these data represents the correct crystallography of Ge-Te.

Figure 10 shows the trigonal system of Ge-Te. Here, both DFT and experimentally obtained data are used as reference. The rhombohedral lattice was found from both DFT and experimental data. DFT resulted in the lattice parameters to be $a = 6.07717\mathring{A}$ and $\gamma = 87.1492°$. However, the data obtained from experiments resulted in the lattice parameters to be $a = 5.99996\mathring{A}$ and $\gamma = 88.561°$. This difference is due to the temperature variation. Mainly, DFT is at 0 K while experiments are usually at room temperature. Despite the differences, we have shown that Ge-Te is both rhombohedral and hexagonal because it belongs to the space group R3m.

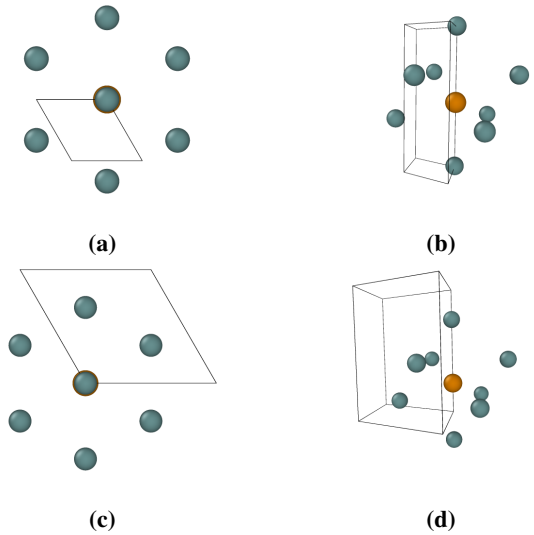

Fig. 10: Visualization of trigonal system of Ge-Te where Ge and Te are represented with grey and orange, respectively. From left to right: (a) and (b) showing the top and perspective view of DFT obtained data, (c) and (d) showing the top and perspective view of experimentally obtained data.

D. Crystallography of Ni-Ti

In the literature, there is still debate on the space group of Ni-Ti R-phase. It has been reported by Naji, Khalil-Allafi, and Khalili [36] that the space group is $P\bar{3}$. However, Xu, Luo, Li, *et al.* [37] claims the space group to be P3. Both papers support their claims with experimental data. Upon further research, it is found that Ni-Ti R-phase can be either P3 or $P\bar{3}$. Otsuka and Ren [4] and Khalil-Allafi, Schmahl, and Toebbens [38] report that assigning space group P3 shows better experimental results, although with subtle differences, compared with $P\bar{3}$. Yet, both papers state that the space group should be considered $P\bar{3}$ since it is more reasonable than P3. This consideration is made since the space group $P\bar{3}$ has a centre of symmetry while the space group P3 does not. Nevertheless, according to the theory of subsection VII-A and VII-B Ni-Ti R-phase

has a trigonal system regardless of the space groups discussed. However, it can only be represented by a hexagonal lattice. Therefore, this report will consider both space groups and compare which is (closest to) a Rhombohedral lattice.

Again, the Wyckoff positions of both space groups are compared to the general Wyckoff positions. The Wyckoff positions for $P\bar{3}$ according to MP are consistent with the Wyckoff positions required for this space group. The atomic arrangement of the cell according to MP do not correspond to the Wyckoff positions for P3. Additionally, the lattice parameters are stated to be $a = 5.39\mathring{A}$, $b = c = 7.25\mathring{A}$, $\alpha = 119.96^\circ$, $\beta = 90.12^\circ$ and $\gamma = 90.04^\circ$. This does not represent a hexagonal lattice while Ni-Ti R-phase should at least be hexagonal. Therefore, we can ignore the data for P3 since it it not representative for the crystallography of Ni-Ti R-phase.

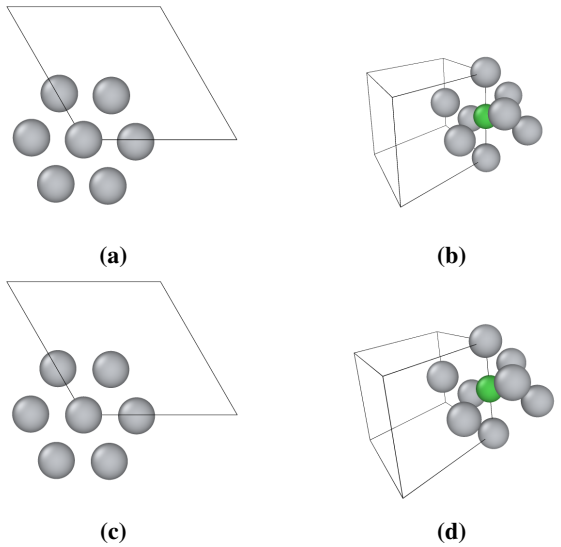

Fig. 11: Visualization of trigonal system of Ni-Ti with space group $P\bar{3}$ where Ni and Ti are represented with green and grey, respectively. From left to right: (a) and (b) show the top and perspective view of DFT obtained data, (c) and (d) show the top and perspective view of experimentally obtained data.

Figure 11 shows the trigonal system of Ni-Ti with the space group $P\bar{3}$. Again, both DFT and experimental data are used as a reference. Shown in Figure 11 (b) and (d), we tried to obtain the rhombohedral Bravais lattice. Based on these Figures it may seem that Ni-Ti is rhombohedral. However, the lattice parameter of the rhombohedral symmetry are not consistent with experiments anymore. DFT resulted in the lattice parameters to be $a = b = 2.93009\mathring{A}$, $c = 3.07355\mathring{A}$, $\alpha = \beta = 89.8098^\circ$ and $\gamma = 92.8677^\circ$. Experimental data showed similar results with $a = b = 3.06981\mathring{A}$, $c = 3.08302\mathring{A}$, $\alpha = \beta = 89.2502^\circ$ and $\gamma = 90.9985^\circ$. This shows that Ni-Ti R-phase is not rhombohedral. However, experimental data is close to a rhombohedral, since the difference between both lattice lengths and angles is smaller compared to DFT. Yet, approximating Ni-Ti as a rhombohedral Bravais lattice might result in inaccurate predictions of the twinning systems, since small angle discrepancies of the lattice angle can lead to significant differences in lattice shear (subsection VI-B).

VIII. Conclusion

In this work, we have studied the the crystal structure of Ni-Ti R-phase and Ge-Te. Guided by EMT [8], the twinning systems that forms upon MT in both alloys have been compared. We found that Ni-Ti and Ge-Te R-phases form similar compound twinning systems during MT from cubic austenite to rhombohedral martensite. It is shown that, despite varying lattice parameters, all materials undergoing the same MT form the twinning systems $\{100\}\langle 110\rangle$ and $\{110\}\langle 100\rangle$. However, it was found that the lattice shear depends strongly on the lattice angle, mainly the lattice shear for Ge-Te was significantly larger than Ni-Ti R-phase in spite of the small difference in the lattice angle. A larger lattice shear might induce plastic deformation and hence hinder SME in GeTe, compared with NiTi. Since the atomic arrangements inside the crystal cells are neglected by EMT, the crystallography of both alloys is studied. This showed that the crystal structure is significantly different and that Ni-Ti is only approximately R-phase, with possible implications on the twin structure, lattice shear and twinning systems.

To conclude, crystallographic theories such as EMT are not sufficient to explain the SME, despite showing significant differences in the lattice shear magnitude. Furthermore, it was shown that Ni-Ti is not rhombohedral despite contradicting claims in previous studies [5], [6], [12], [17]. In fact, the SME is also related to atomic-scale mechanisms. Therefore, atomic mechanisms cannot be neglected when studying the SME and a different crystallography might induce a different twinning system structure and mobility.

Atomistic models such as Molecular Dynamics consider atomic mechanism. By modeling the interface between twins, the motion of the twin can be observed after applying an external load (shear or temperature). This will help to further investigate the impact of the different crystal structures of GeTe and NiTi on the SME effect.

References

[1] K. Otsuka and C. M. Wayman, *Shape memory materials*. Cambridge university press, 1999.

[2] J. M. Jani, M. Leary, A. Subic, and M. A. Gibson, "A review of shape memory alloy research, applications and opportunities," *Materials & Design (1980-2015)*, vol. 56, pp. 1078–1113, 2014.

[3] K. Otsuka and T. Kakeshita, "Science and technology of shape-memory alloys: New developments," *mrs bulletin*, vol. 27, no. 2, pp. 91–100, 2002.

[4] K. Otsuka and X. Ren, "Physical metallurgy of ti–ni-based shape memory alloys," *Progress in materials science*, vol. 50, no. 5, pp. 511–678, 2005.

[5] X. Zhang and H. Sehitoglu, "Crystallography of the b2→ r→ b19 phase transformations in niti," *Materials Science and Engineering: A*, vol. 374, no. 1-2, pp. 292–302, 2004.

[6] K. Bhattacharya and *et al.*, *Microstructure of martensite: why it forms and how it gives rise to the shape-memory effect*. Oxford University Press, 2003, vol. 2.

[7] P. A. Vermeulen, A. Kumar, G. H. ten Brink, G. R. Blake, and B. J. Kooi, "Unravelling the domain structures in gete and laalo3," *Crystal Growth & Design*, vol. 16, no. 10, pp. 5915–5922, 2016.

[8] J. M. Ball and R. D. James, "Fine phase mixtures as minimizers of energy," *Archive for Rational Mechanics and Analysis*, vol. 100, pp. 13–52, 1987.

[9] H. Bhadeshia and C. Wayman, "Phase transformations: Nondiffusive," in *Physical metallurgy*, Elsevier, 2014, pp. 1021–1072.

[10] T. Waitz, "The self-accommodated morphology of martensite in nanocrystalline niti shape memory alloys," *Acta Materialia*, vol. 53, no. 8, pp. 2273–2283, 2005.

[11] Y. Song, X. Chen, V. Dabade, T. W. Shield, and R. D. James, "Enhanced reversibility and unusual microstructure of a phase-transforming material," *Nature*, vol. 502, no. 7469, pp. 85–88, 2013.

[12] K. F. Hane and T. W. Shield, "Microstructure in the cubic to trigonal transition," *Materials Science and Engineering: A*, vol. 291, no. 1-2, pp. 147–159, 2000.

[13] K. Bhattacharya, "Self-accommodation in martensite," *Archive for rational mechanics and analysis*, vol. 120, pp. 201–244, 1992.

[14] B. A. Bilby and A. Crocker, "The theory of the crystallography of deformation twinning," *Proceedings of the Royal Society of London. Series A. Mathematical and physical sciences*, vol. 288, no. 1413, pp. 240–255, 1965.

[15] S. Prokoshkin, A. Korotitskiy, V. Brailovski, S. Turenne, I. Y. Khmelevskaya, and I. Trubitsyna, "On the lattice parameters of phases in binary ti–ni shape memory alloys," *Acta Materialia*, vol. 52, no. 15, pp. 4479–4492, 2004.

[16] L. La Rosa and F. Maresca, "On the impact of lattice parameter accuracy of atomistic simulations on the microstructure of ni–ti shape memory alloys," *Modelling and Simulation in Materials Science and Engineering*, vol. 30, no. 1, p. 014 003, 2021.

[17] R. D. James and K. F. Hane, "Martensitic transformations and shape-memory materials," *Acta materialia*, vol. 48, no. 1, pp. 197–222, 2000.

[18] S. Miyazaki and C. Wayman, "The r-phase transition and associated shape memory mechanism in ti-ni single crystals," *Acta metallurgica*, vol. 36, no. 1, pp. 181–192, 1988.

[19] M. B. Bjerke and R. Renger, "Being smart about writing smart objectives," *Evaluation and program planning*, vol. 61, pp. 125–127, 2017.

[20] P. Verschuren, H. Doorewaard, and M. Mellion, *Designing a research project*. Eleven International Publishing The Hague, 2010, vol. 2.

[21] K. F. Hane and T. W. Shield, "Symmetry and microstructure in martensites," *Philosophical Magazine A*, vol. 78, no. 6, pp. 1215–1252, 1998.

[22] H. S. Lee, B.-S. Kim, C.-W. Cho, *et al.*, "Herringbone structure in gete-based thermoelectric materials," *Acta Materialia*, vol. 91, pp. 83–90, 2015.

[23] J. Stoemenos and R. Vincent, "Twining faults in epitaxial films of germanium telluride and gete snte alloys," *physica status solidi (a)*, vol. 11, no. 2, pp. 545–558, 1972.

[24] M. Nespolo, "Introduction to crystallography. by frank hoffmann. springer, 2020. hardback, pp. x+ 309. price gbp 59.99. isbn 9783030351090.," *Acta Crystallographica Section A: Foundations and Advances*, vol. 77, no. 3, pp. 235–238, 2021.

[25] M. Pitteri and G. Zanzotto, "On the definition and classification of bravais lattices," *Acta Crys-*

tallographica Section A: Foundations of Crystallography, vol. 52, no. 6, pp. 830–838, 1996.

[26] M. Nespolo, M. I. Aroyo, and B. Souvignier, "Crystallographic shelves: Space-group hierarchy explained," *Journal of Applied Crystallography*, vol. 51, no. 5, pp. 1481–1491, 2018.

[27] T. Hahn, H. Klapper, U. Müller, and M. Aroyo, "Point groups and crystal classes," 2016.

[28] A. Janner, T. Janssen, and P. De Wolff, "Wyckoff positions used for the classification of bravais classes of modulated crystals," *Acta Crystallographica Section A: Foundations of Crystallography*, vol. 39, no. 5, pp. 667–670, 1983.

[29] M. I. Aroyo, J. M. Perez-Mato, D. Orobengoa, E. Tasci, G. de la Flor, and A. Kirov, "Crystallography online: Bilbao crystallographic server," *Bulg. Chem. Commun*, vol. 43, no. 2, pp. 183–197, 2011.

[30] M. I. Aroyo, J. M. Perez-Mato, C. Capillas, *et al.*, *Zeitschrift für Kristallographie - Crystalline Materials*, vol. 221, no. 1, pp. 15–27, 2006.

[31] M. I. Aroyo, A. Kirov, C. Capillas, J. M. Perez-Mato, and H. Wondratschek, "Bilbao Crystallographic Server. II. Representations of crystallographic point groups and space groups," *Acta Crystallographica Section A*, vol. 62, no. 2, pp. 115–128, Mar. 2006.

[32] T. Chattopadhyay, J. Boucherle, *et al.*, "Neutron diffraction study on the structural phase transition in gete," *Journal of Physics C: Solid State Physics*, vol. 20, no. 10, p. 1431, 1987.

[33] A. Jain, S. P. Ong, G. Hautier, *et al.*, "Commentary: The materials project: A materials genome approach to accelerating materials innovation," *APL materials*, vol. 1, no. 1, p. 011 002, 2013.

[34] A. Stukowski, "Visualization and analysis of atomistic simulation data with OVITO-the Open Visualization Tool," *MODELLING AND SIMULATION IN MATERIALS SCIENCE AND ENGINEERING*, vol. 18, no. 1, JAN 2010, ISSN: 0965-0393.

[35] S. Gražulis, D. Chateigner, R. T. Downs, *et al.*, "Crystallography open database–an open-access collection of crystal structures," *Journal of applied crystallography*, vol. 42, no. 4, pp. 726–729, 2009.

[36] H. Naji, J. Khalil-Allafi, and V. Khalili, "Microstructural characterization and quantitative phase analysis of ni-rich niti after stress assisted aging for long times using the rietveld method," *Materials Chemistry and Physics*, vol. 241, p. 122 317, 2020.

[37] K. Xu, J. Luo, C. Li, *et al.*, "Mechanisms of stress-induced martensitic transformation and transformation-induced plasticity in niti shape memory alloy related to superelastic stability," *Scripta Materialia*, vol. 217, p. 114 775, 2022.

[38] J. Khalil-Allafi, W. W. Schmahl, and D. Toebbens, "Space group and crystal structure of the r-phase in binary niti shape memory alloys," *Acta materialia*, vol. 54, no. 12, pp. 3171–3175, 2006.

```
1
2  function [Twinning_systems_reference, Twinning_systems_current] =
       R_phase_twinning_systems(gamma,a0)
3  % MATLAB script file for the analysis of the twinning systems in R-phase
4  % crystal structures. This script can describe crystallographic
5  % features of the martensitic transformation of R-phase crystals, such as
6  % twin variants.
7
8  % Here the martensitic transformation is between the B2 (bcc) austenite
9  % phase and the R-phase (Rhombohedral) martensite
10
11 % The twinning equation is solved by using MALLARD's LAW
12
13 % Experimental lattice angle:
14 % S. Miyazaki and C. Wayman (1988) lattice angle experiment Ni-Ti R-phase:
       gamma= approx. 89.5 degrees
15 % P. A. Vermeulen et al. (2016) Crystollographic structure experiment Ge-Te:
        gamma approx. 82.4 degrees
16
17 % Ayoub Chahbari, May 2023
18
19 format short
20 %% Set the cartesian frame in amstrongs and lattice angle in degrees
21
22 i=[1 0 0]';
23 j=[0 1 0]';
24 k=[0 0 1]';
25 %% Define the symmetry operations
26 %%% Define the point group of the cubic crystal structure
27
28 R1=eye(3,3);
29 R2=rotx(90);R9=rotx(180);R22=rotx(270);
30 R3=roty(90);R10=roty(180);R23=roty(270);
31 R4=rotz(90);R11=rotz(180);R24=rotz(270);
32
33 axang=[1/sqrt(3) 1/sqrt(3) 1/sqrt(3) 2*pi/3];
34 R5=axang2rotm(axang);
35
36 axang=[1/sqrt(3) 1/sqrt(3) -1/sqrt(3) 2*pi/3];
37 R6=axang2rotm(axang);
38
39 axang=[1/sqrt(3) -1/sqrt(3) 1/sqrt(3) 2*pi/3];
40 R7=axang2rotm(axang);
41
42 axang=[-1/sqrt(3) 1/sqrt(3) 1/sqrt(3) 2*pi/3];
43 R8=axang2rotm(axang);
44
45 axang=[1/sqrt(2) 1/sqrt(2) 0 pi];
```

```
R12=axang2rotm(axang);

axang=[1/sqrt(2) -1/sqrt(2) 0 pi];
R13=axang2rotm(axang);

axang=[0 1/sqrt(2) 1/sqrt(2) pi];
R14=axang2rotm(axang);

axang=[0 1/sqrt(2) -1/sqrt(2) pi];
R15=axang2rotm(axang);

axang=[1/sqrt(2) 0 1/sqrt(2) pi];
R16=axang2rotm(axang);

axang=[-1/sqrt(2) 0 1/sqrt(2) pi];
R17=axang2rotm(axang);

axang=[1/sqrt(3) 1/sqrt(3) 1/sqrt(3) 4*pi/3];
R18=axang2rotm(axang);

axang=[1/sqrt(3) 1/sqrt(3) -1/sqrt(3) 4*pi/3];
R19=axang2rotm(axang);

axang=[1/sqrt(3) -1/sqrt(3) 1/sqrt(3) 4*pi/3];
R20=axang2rotm(axang);

axang=[-1/sqrt(3) 1/sqrt(3) 1/sqrt(3) 4*pi/3];
R21=axang2rotm(axang);

%%% Store all 24 point groups
R={R1; R2; R3; R4; R5; R6; R7; R8; R9; R10; R11; R12; R13; R14; R15; R16;
   R17; R18; R19; R20; R21; R22; R23; R24};

n=24 ;
 for m = 1:n
     R{m}=round(R{m},5);
 end

cubrot=24;

%%% Define the point group of the Rhombohedral crystal structure
r1=R1; r2=R9; r3=rotz(120); r4=rotz(240);
r5=axang2rotm([1/2 sqrt(3)/2 0 pi]);
r6=axang2rotm([-1/2 sqrt(3)/2 0 pi]);

rhomrot=6;

%%% Define the number of variants
N=cubrot/rhomrot;
%% Martensitic transformation
```

```
disp('Computing the Bain Strain...')

%%% Set the face-centered austenite lattice basis
fa1=a0*i;
fa2=a0*j;
fa3=a0*k;

FB2F=[fa1 fa2 fa3];

%%% Set the face-centered martensite lattice basis
fm1=a0*(sind(gamma/2)*i-sind(gamma/2)/sqrt(3)*j+sqrt((4*(cosd(gamma/2))^2-1)
   /3)*k);
fm2=a0*((2*sind(gamma/2))/sqrt(3)*j+sqrt((4*(cosd(gamma/2))^2-1)/3)*k);
fm3=a0*(-sind(gamma/2)*i-sind(gamma/2)/sqrt(3)*j+sqrt((4*(cosd(gamma/2))
   ^2-1)/3)*k);

FRF=[fm1 fm2 fm3];

%%% Compute the deformation gradient
F=FRF/FB2F;
DeltaV=det(F);

%%% Compute the Bain Strain
C=F'*F;
[V,D]=eig(C);

B=sqrt(D(1,1))*V(:,1)*V(:,1)'+sqrt(D(2,2))*V(:,2)*V(:,2)'+sqrt(D(3,3))*V
   (:,3)*V(:,3)';
%% Define entries Bain matrices
alpha=(sqrt(1+2*cosd(gamma))+2*sqrt(1-cosd(gamma)))/3;
delta=(sqrt(1+2*cosd(gamma))-sqrt(1-cosd(gamma)))/3;

%alpha=round(alpha1,5);
%delta=round(delta1,5);

%%% Construct Bain matrices
U1=[alpha delta delta; delta alpha delta; delta delta alpha];
U2=R9'*U1*R9;
U3=R11'*U1*R11;
U4=R10'*U1*R10;
Q={F/U1; F/U2; F/U3; F/U4};
%% Compute the twins formed by U1 and U2, R(i,180)

disp('Computing twins formed by martensite variants 1-2, R(i,180) ...')

%%% Determine Type 1 twin
a1=2*((inv(U1)'*i)/norm(inv(U1)'*i)^2 -U1*i);
n1=i;
s1=[norm(a1)*norm(U1\n1) nan nan]';

```

```
shear1=a1*1/a1(2);
plane1=n1';

%%% Transform back to current configuration
eta1=inv(FRF)*((Q{1}*a1)/norm(Q{1}*a1));
K1=((n1'*inv(F))/norm(n1'*inv(F))*FRF)';

T1=[s1 shear1 n1 eta1/eta1(2) K1/K1(1)];

%%% Determine whether conforms to habit plane conditions
mu1=plane1*U1*((U1*U1-eye(3,3))\eye(3,3))*a1;
eta1=trace(U1*U1)-det(U1*U1)-2+(norm(a1)^2)/(2*mu1);

%%% Determine Type 2 twin
n2=2*(i-(U1'*U1*i)/norm(U1*i)^2);
norm2=norm(n2);
n2=n2/norm2;
a2=norm2*U1*i;

shear2=a2*1/a2(1);
plane2=n2';

%%% Transform back to current configuration
eta2=inv(FRF)*((Q{1}*a2)/norm(Q{1}*a2));
K2=((n2'*inv(F))/norm(n2'*inv(F))*FRF)';

T2=[s1 shear2 2*n2/sqrt(2) eta2/eta2(1) K2/K2(2)];

%%% Determine whether conforms to habit plane conditions
mu2=plane2*U1*((U1*U1-eye(3,3))\eye(3,3))*a2;
eta2=trace(U1*U1)-det(U1*U1)-2+(norm(a2)^2)/(2*mu2);
%% Compute the twins formed by U2 and U1, R(i,180)

disp('Computing twins formed by martensite variants 2-1, R(i,180) ...')

%%% Determine Type 1 twin
a1=2*((inv(U2)'*i)/norm(inv(U2)'*i)^2 -U2*i);
n1=i;
s2=[norm(a1)*norm(U2\n1) nan nan]';

shear1=a1*1/a1(2);
plane1=n1';

%%% Transform back to current configuration
eta1=inv(FRF)*((Q{2}*a1)/norm(Q{2}*a1));
K1=((n1'*inv(F))/norm(n1'*inv(F))*FRF)';

T3=[s2 shear1 n1 eta1/eta1(2) K1/K1(1)];

%%% Determine Type 2 twin
```

```
n2=2*(i-(U2'*U2*i)/norm(U2*i)^2);
norm2=norm(n2);
n2=n2/norm2;
a2=norm2*U2*i;

shear2=a2*1/a2(1);
plane2=n2';

%%% Transform back to current configuration
eta2=inv(FRF)*((Q{2}*a2)/norm(Q{2}*a2));
K2=((n2'*inv(F))/norm(n2'*inv(F))*FRF)';

T4=[s2 shear2 2*n2/sqrt(2) eta2/eta2(1) K2/K2(2)];
%% Compute the twins formed by U1 and U3, R(k,180)

disp('Computing twins formed by martensite variants 1-3, R(k,180) ...')

%%% Determine Type 1 twin
a1=2*((inv(U1)'*k)/norm(inv(U1)'*k)^2 -U1*k);
n1=k;
s3=[norm(a1)*norm(U1\n1) nan nan]';

shear1=a1*1/a1(2);
plane1=n1';

%%% Transform back to current configuration
eta1=inv(FRF)*((Q{1}*a1)/norm(Q{1}*a1));
K1=((n1'*inv(F))/norm(n1'*inv(F))*FRF)';

T5=[s3 shear1 n1 eta1/eta1(1) K1/K1(3)];

%%% Determine Type 2 twin
n2=2*(k-(U1'*U1*k)/norm(U1*k)^2);
norm2=norm(n2);
n2=n2/norm2;
a2=norm2*U1*k;

shear2=a2*1/a2(3);
plane2=n2';

%%% Transform back to current configuration
eta2=inv(FRF)*((Q{1}*a2)/norm(Q{1}*a2));
K2=((n2'*inv(F))/norm(n2'*inv(F))*FRF)';

T6=[s3 shear2 2*n2/sqrt(2) eta2/eta2(3) K2/K2(1)];
%% Compute the twins formed by U3 and U1, R(k,180)

disp('Computing twins formed by martensite variants 3-1, R(k,180) ...')

%%% Determine Type 1 twin
```

```
a1=2*((inv(U3)'*k)/norm(inv(U3)'*k)^2 -U3*k);
n1=k;
s4=[norm(a1)*norm(U3\n1) nan nan]';

shear1=a1*1/a1(2);
plane1=n1';

%%% Transform back to current configuration
eta1=inv(FRF)*((Q{3}*a1)/norm(Q{3}*a1));
K1=((n1'*inv(F))/norm(n1'*inv(F))*FRF)';

T7=[s4 shear1 n1 eta1/eta1(1) K1/K1(3)];

%%% Determine Type 2 twin
n2=2*(k-(U3'*U3*k)/norm(U3*k)^2);
norm2=norm(n2);
n2=n2/norm2;
a2=norm2*U3*k;

shear2=a2*1/a2(3);
plane2=n2';

%%% Transform back to current configuration
eta2=inv(FRF)*((Q{3}*a2)/norm(Q{3}*a2));
K2=((n2'*inv(F))/norm(n2'*inv(F))*FRF)';

T8=[s4 shear2 2*n2/sqrt(2) eta2/eta2(3) K2/K2(1)];
%% Compute the twins formed by U1 and U4, R(j,180)

disp('Computing twins formed by martensite variants 1-4, R(j,180) ...')

%%% Determine Type 1 twin
a1=2*((inv(U1)'*j)/norm(inv(U1)'*j)^2 -U1*j);
n1=j;
s5=[norm(a1)*norm(U1\n1) nan nan]';

shear1=a1*1/a1(1);
plane1=n1';

%%% Transform back to current configuration
eta1=inv(FRF)*((Q{1}*a1)/norm(Q{1}*a1));
K1=((n1'*inv(F))/norm(n1'*inv(F))*FRF)';

T9=[s5 shear1 n1 eta1/eta1(1) K1/K1(2)];

%%% Determine Type 2 twin
n2=2*(j-(U1'*U1*j)/norm(U1*j)^2);
norm2=norm(n2);
n2=n2/norm2;
a2=norm2*U1*j;
```

```
292
293 shear2=a2*1/a2(2);
294 plane2=n2';
295
296 %%% Transform back to current configuration
297 eta2=inv(FRF)*((Q{1}*a2)/norm(Q{1}*a2));
298 K2=((n2'*inv(F))/norm(n2'*inv(F))*FRF)';
299
300 T10=[s5 shear2 2*n2/sqrt(2) eta2/eta2(2) K2/K2(1)];
301 %% Compute the twins formed by U4 and U1, R(j,180)
302
303 disp('Computing twins formed by martensite variants 4-1, R(j,180) ...')
304
305 %%% Determine Type 1 twin
306 a1=2*((inv(U4)'*j)/norm(inv(U4)'*j)^2 -U4*j);
307 n1=j;
308 s6=[norm(a1)*norm(U4\n1) nan nan]';
309
310 shear1=a1*1/a1(1);
311 plane1=n1';
312
313 %%% Transform back to current configuration
314 eta1=inv(FRF)*((Q{4}*a1)/norm(Q{4}*a1));
315 K1=((n1'*inv(F))/norm(n1'*inv(F))*FRF)';
316
317 T11=[s6 shear1 n1 eta1/eta1(1) K1/K1(2)];
318
319 %%% Determine Type 2 twin
320 n2=2*(j-(U4'*U4*j)/norm(U4*j)^2);
321 norm2=norm(n2);
322 n2=n2/norm2;
323 a2=norm2*U4*j;
324
325 shear2=a2*1/a2(2);
326 plane2=n2';
327
328 %%% Transform back to current configuration
329 eta2=inv(FRF)*((Q{4}*a2)/norm(Q{4}*a2));
330 K2=((n2'*inv(F))/norm(n2'*inv(F))*FRF)';
331
332 T12=[s6 shear2 2*n2/sqrt(2) eta2/eta2(2) K2/K2(1)];
333 %% Compute the twins formed by U2 and U3, R(j,180)
334
335 disp('Computing twins formed by martensite variants 2-3, R(j,180) ...')
336
337 %%% Determine Type 1 twin
338 a1=2*((inv(U2)'*j)/norm(inv(U2)'*j)^2 -U2*j);
339 n1=j;
340 s7=[norm(a1)*norm(U2\n1) nan nan]';
341
```

```
shear1=a1*1/a1(3);
plane1=n1';

%%% Transform back to current configuration
eta1=inv(FRF)*((Q{2}*a1)/norm(Q{2}*a1));
K1=((n1'*inv(F))/norm(n1'*inv(F))*FRF)';

T13=[s7 shear1 n1 eta1/eta1(1) K1/K1(2)];

%%% Determine Type 2 twin
n2=2*(j-(U2'*U2*j)/norm(U2*j)^2);
norm2=norm(n2);
n2=n2/norm2;
a2=norm2*U2*j;

shear2=a2*1/a2(2);
plane2=n2';

%%% Transform back to current configuration
eta2=inv(FRF)*((Q{2}*a2)/norm(Q{2}*a2));
K2=((n2'*inv(F))/norm(n2'*inv(F))*FRF)';

T14=[s7 shear2 2*n2/sqrt(2) eta2/eta2(2) K2/K2(1)];
%% Compute the twins formed by U3 and U2, R(j,180)

disp('Computing twins formed by martensite variants 3-2, R(j,180) ...')

%%% Determine Type 1 twin
a1=2*((inv(U3)'*j)/norm(inv(U3)'*j)^2 -U3*j);
n1=j;
s8=[norm(a1)*norm(U3\n1) nan nan]';

shear1=a1*1/a1(1);
plane1=n1';

%%% Transform back to current configuration
eta1=inv(FRF)*((Q{3}*a1)/norm(Q{3}*a1));
K1=((n1'*inv(F))/norm(n1'*inv(F))*FRF)';

T15=[s8 shear1 n1 eta1/eta1(1) K1/K1(2)];

%%% Determine Type 2 twin
n2=2*(j-(U3'*U3*j)/norm(U3*j)^2);
norm2=norm(n2);
n2=n2/norm2;
a2=norm2*U3*j;

shear2=a2*1/a2(2);
plane2=n2';

```

```
%%% Transform back to current configuration
eta2=inv(FRF)*((Q{3}*a2)/norm(Q{3}*a2));
K2=((n2'*inv(F))/norm(n2'*inv(F))*FRF)';

T16=[s8 shear2 2*n2/sqrt(2) eta2/eta2(2) K2/K2(1)];
%% Compute the twins formed by U2 and U4, R(k,180)

disp('Computing twins formed by martensite variants 2-4, R(k,180) ...')

%%% Determine Type 1 twin
a1=2*((inv(U2)'*k)/norm(inv(U2)'*k)^2 -U2*k);
n1=k;
s9=[norm(a1)*norm(U2\n1) nan nan]';

shear1=a1*1/a1(2);
plane1=n1';

%%% Transform back to current configuration
eta1=inv(FRF)*((Q{2}*a1)/norm(Q{2}*a1));
K1=((n1'*inv(F))/norm(n1'*inv(F))*FRF)';

T17=[s9 shear1 n1 eta1/eta1(1) K1/K1(3)];

%%% Determine Type 2 twin
n2=2*(k-(U2'*U2*k)/norm(U2*k)^2);
norm2=norm(n2);
n2=n2/norm2;
a2=norm2*U2*k;

shear2=a2*1/a2(3);
plane2=n2';

%%% Transform back to current configuration
eta2=inv(FRF)*((Q{2}*a2)/norm(Q{2}*a2));
K2=((n2'*inv(F))/norm(n2'*inv(F))*FRF)';

T18=[s9 shear2 2*n2/sqrt(2) eta2/eta2(3) K2/K2(1)];
%% Compute the twins formed by U4 and U2, R(k,180)

disp('Computing twins formed by martensite variants 4-2, R(k,180) ...')

%%% Determine Type 1 twin
a1=2*((inv(U4)'*k)/norm(inv(U4)'*k)^2 -U4*k);
n1=k;
s10=[norm(a1)*norm(U4\n1) nan nan]';

shear1=a1*1/a1(1);
plane1=n1';

%%% Transform back to current configuration
```

```
eta1=inv(FRF)*((Q{4}*a1)/norm(Q{4}*a1));
K1=((n1'*inv(F))/norm(n1'*inv(F))*FRF)';

T19=[s10 shear1 n1 eta1/eta1(1) K1/K1(3)];

%%% Determine Type 2 twin
n2=2*(k-(U4'*U4*k)/norm(U4*k)^2);
norm2=norm(n2);
n2=n2/norm2;
a2=norm2*U4*k;

shear2=a2*1/a2(3);
plane2=n2';

%%% Transform back to current configuration
eta2=inv(FRF)*((Q{4}*a2)/norm(Q{4}*a2));
K2=((n2'*inv(F))/norm(n2'*inv(F))*FRF)';

T20=[s10 shear2 2*n2/sqrt(2) eta2/eta2(3) K2/K2(1)];
%% Compute the twins formed by U3 and U4, R(i,180)

disp('Computing twins formed by martensite variants 3-4, R(i,180) ...')

%%% Determine Type 1 twin
a1=2*((inv(U3)'*i)/norm(inv(U3)'*i)^2 -U3*i);
n1=i;
s11=[norm(a1)*norm(U3\n1) nan nan]';

shear1=a1*1/a1(2);
plane1=n1';

%%% Transform back to current configuration
eta1=inv(FRF)*((Q{3}*a1)/norm(Q{3}*a1));
K1=((n1'*inv(F))/norm(n1'*inv(F))*FRF)';

T21=[s11 shear1 n1 eta1/eta1(2) K1/K1(1)];

%%% Determine Type 2 twin
n2=2*(i-(U3'*U3*i)/norm(U3*i)^2);
norm2=norm(n2);
n2=n2/norm2;
a2=norm2*U3*i;

shear2=a2*1/a2(1);
plane2=n2';

%%% Transform back to current configuration
eta2=inv(FRF)*((Q{3}*a2)/norm(Q{3}*a2));
K2=((n2'*inv(F))/norm(n2'*inv(F))*FRF)';

```

```
T22=[s11 shear2 2*n2/sqrt(2) eta2/eta2(1) K2/K2(2)];
%% Compute the twins formed by U4 and U3, R(i,180)

disp('Computing twins formed by martensite variants 4-3, R(i,180) ...')

%%% Determine Type 1 twin
a1=2*((inv(U4)'*i)/norm(inv(U4)'*i)^2 -U4*i);
n1=i;
s12=[norm(a1)*norm(U4\n1) nan nan]';

shear1=a1*1/a1(3);
plane1=n1';

%%% Transform back to current configuration
eta1=inv(FRF)*((Q{4}*a1)/norm(Q{4}*a1));
K1=((n1'*inv(F))/norm(n1'*inv(F))*FRF)';

T23=[s12 shear1 n1 eta1/eta1(2) K1/K1(1)];

%%% Determine Type 2 twin
n2=2*(i-(U4'*U4*i)/norm(U4*i)^2);
norm2=norm(n2);
n2=n2/norm2;
a2=norm2*U4*i;

shear2=a2*1/a2(1);
plane2=n2';

%%% Transform back to current configuration
eta2=inv(FRF)*((Q{4}*a2)/norm(Q{4}*a2));
K2=((n2'*inv(F))/norm(n2'*inv(F))*FRF)';

T24=[s12 shear2 2*n2/sqrt(2) eta2/eta2(1) K2/K2(2)];
%% Create table summarizing twinning systems
%%% Create table with respect to reference configuration
twinning_mode =
   ["1-2";"2-1";"1-3";"3-1";"1-4";"4-1";"2-3";"3-2";"2-4";"4-2";"3-4";"4-3"];

n1 = round([T1(:,3)'; T3(:,3)'; T5(:,3)'; T7(:,3)'; T9(:,3)'; T11(:,3)'; T13
   (:,3)'; T15(:,3)'; T17(:,3)'; T19(:,3)'; T21(:,3)'; T23(:,3)'],10);
a1 = round([T1(:,2)'; T3(:,2)'; T5(:,2)'; T7(:,2)'; T9(:,2)'; T11(:,2)'; T13
   (:,2)'; T15(:,2)'; T17(:,2)'; T19(:,2)'; T21(:,2)'; T23(:,2)'],10);
n2 = round([T2(:,3)'; T4(:,3)'; T6(:,3)'; T8(:,3)'; T10(:,3)'; T12(:,3)';
   T14(:,3)'; T16(:,3)'; T18(:,3)'; T20(:,3)'; T22(:,3)'; T24(:,3)'],10);
a2 = round([T2(:,2)'; T4(:,2)'; T6(:,2)'; T8(:,2)'; T10(:,2)'; T12(:,2)';
   T14(:,2)'; T16(:,2)'; T18(:,2)'; T20(:,2)'; T22(:,2)'; T24(:,2)'],10);
shear  = round([s1(1); s2(1); s3(1); s4(1); s5(1); s6(1); s7(1); s8(1); s9
   (1); s10(1); s11(1); s12(1)],10);

Twinning_systems_reference = table(twinning_mode,n1,a1,n2,a2,shear)
```

```
535
536 %%% Create table with respect to current configuration
537 twinning_mode =
       ["1-2";"2-1";"1-3";"3-1";"1-4";"4-1";"2-3";"3-2";"2-4";"4-2";"3-4";"4-3"];

538 eta1 = round([T1(:,4)'; T3(:,4)'; T5(:,4)'; T7(:,4)'; T9(:,4)'; T11(:,4)';
       T13(:,4)'; T15(:,4)'; T17(:,4)'; T19(:,4)'; T21(:,4)'; T23(:,4)'],10);
539 K1 = round([T1(:,5)'; T3(:,5)'; T5(:,5)'; T7(:,5)'; T9(:,5)'; T11(:,5)'; T13
       (:,5)'; T15(:,5)'; T17(:,5)'; T19(:,5)'; T21(:,5)'; T23(:,5)'],10);
540 eta2 = round([T2(:,4)'; T4(:,4)'; T6(:,4)'; T8(:,4)'; T10(:,4)'; T12(:,4)';
       T14(:,4)'; T16(:,4)'; T18(:,4)'; T20(:,4)'; T22(:,4)'; T24(:,4)'],10);
541 K2 = round([T2(:,5)'; T4(:,5)'; T6(:,5)'; T8(:,5)'; T10(:,5)'; T12(:,5)';
       T14(:,5)'; T16(:,5)'; T18(:,5)'; T20(:,5)'; T22(:,5)'; T24(:,5)'],10);
542 shear  = round([s1(1); s2(1); s3(1); s4(1); s5(1); s6(1); s7(1); s8(1); s9
       (1); s10(1); s11(1); s12(1)],10);
543
544 Twinning_systems_current = table(twinning_mode,eta1,K1,eta2,K2,shear)
545
546 %%% Display possibility of Twin based on habit plane equation
547 if mu1<=-2 && mu2<=-2 && eta1>=0 && eta2>=0
548     disp('Both planes meet both conditions, so Twinning systems are {1 0
          0}<0 1 1> and {1 1 0}<0 0 1>')
549 elseif mu1>-2 && mu2<=-2
550     disp('Only {1 1 0} plane meets both conditions, so Twinning system is {1
           1 0}<0 0 1>')
551 elseif mu1<=-2 && mu2>-2
552     disp('Only {1 0 0} plane meets both conditions, so Twinning system is {1
           0 0}<0 1 1>')
553 elseif mu1<=-2 && mu2<=-2 && eta1<0
554     disp('Only {1 1 0} plane meets both conditions, so Twinning system is {1
           1 0}<0 0 1>')
555 elseif mu1<=-2 && mu2<=-2 && eta2<0
556     disp('Only {1 0 0} plane meets both conditions, so Twinning system is {1
           0 0}<0 1 1>')
557 end
558 end
```